

UKAEA-CCFE-PR(23)110

M. J. Lloyd, C. Teoh, G. Lim, D. Nguyen-Manh, D.  
Sobieraj, J. S. Wrobel, R. E. Simpson

# **Increasing the Adhesion of W to Si Substrates using Cr/Ti Interlayers**

Enquiries about copyright and reproduction should in the first instance be addressed to the UKAEA Publications Officer, Culham Science Centre, Building K1/O/83 Abingdon, Oxfordshire, OX14 3DB, UK. The United Kingdom Atomic Energy Authority is the copyright holder.

The contents of this document and all other UKAEA Preprints, Reports and Conference Papers are available to view online free at [scientific-publications.ukaea.uk/](https://scientific-publications.ukaea.uk/)

# **Increasing the Adhesion of W to Si Substrates using Cr/Ti Interlayers**

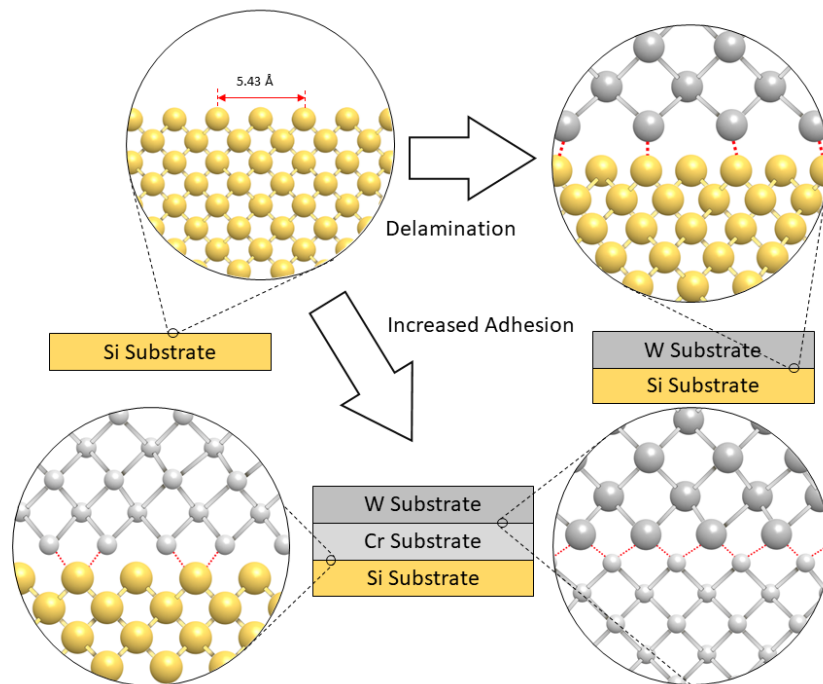
M. J. Lloyd, C. Teoh, G. Lim, D. Nguyen-Manh, D. Sobieraj, J. S.  
Wrobel, R. E. Simpson



# Graphical Abstract

## Increasing the Adhesion of W to Si Substrates using Cr/Ti Interlayers

M. J. Lloyd, C. Teoh, G. Lim, D. Nguyen-Manh, D. Sobieraj, J. S. Wróbel, R. E. Simpson



## Highlights

### **Increasing the Adhesion of W to Si Substrates using Cr/Ti Interlayers**

M. J. Lloyd, C. Teoh, G. Lim, D. Nguyen-Manh, D. Sobieraj, J. S. Wróbel, R. E. Simpson

- Research highlight 1

- Research highlight 2

# Increasing the Adhesion of W to Si Substrates using Cr/Ti Interlayers

M. J. Lloyd<sup>a,1</sup>, C. Teoh<sup>a</sup>, G. Lim<sup>a</sup>, D. Nguyen-Manh<sup>b,c</sup>, D. Sobieraj<sup>d</sup>, J. S. Wróbel<sup>d</sup>, R. E. Simpson<sup>a</sup>

<sup>a</sup>Engineering Product Development, Singapore University of Technology and Design, 8 Somapah Road, Singapore, 487372, Singapore

<sup>b</sup>United Kingdom Atomic Energy Authority, Culham Science Centre, Abingdon, OX14 3DB, United Kingdom

<sup>c</sup>Department of Materials, University of Oxford, Oxford, OX1 3PH, United Kingdom

<sup>d</sup>Faculty of Materials Science and Engineering, Warsaw University of Technology, ul. Wołoska 141, Warsaw, 02-507, Poland

---

## Abstract

The realisation of fusion energy depends on the development of advanced materials for challenging environments. Rapid screening of prototype alloys using magnetron sputtering and high throughput characterisation is currently being applied to candidate W alloys with improved mechanical performance, reduced activation and tolerance to damage from neutron irradiation. Delamination of these films is a barrier to the application of this approach. In this study, delamination of W films was determined to be a result of high compressive residual stresses, and inadequate adhesion to the Si substrate. It was found that using a Ti or Cr interfacial layer increases adhesion, something that was strongly supported by interface W/Cr studies from first-principles calculations based on the Density Functional Theory (DFT). It is shown for all configurations that the interface binding energies between W and Cr are attractive with the W(110)/Cr(110) is predicted to be the most stable with a higher adhesive energy.

*Keywords:* Tungsten chromium alloys, Nuclear fusion, rapid prototyping, Density function theory

---

Alloys of W have been investigated for many years as candidate materials for the plasma facing components (PFCs) of a future nuclear fusion power station. Pure W is the leading candidate material due to its attractive high temperature properties [1, 2] and low activation under neutron irradiation [3, 4]. The properties of W severely degrade when exposed to neutron irradiation, including radiation embrittlement [5–11], an increase in the Ductile to Brittle Transition Temperature (DBTT) [12–16], a reduction of thermal conductivity [17–19], and radiation enhanced recrystallisation [20]. Alloys of W have been investigated to improve key properties, whilst maintaining low activation.

Re has a strong ductilising effect in W and was studied extensively in 1960s and 70s [21–24]. Radiation induced precipitation of Re reverses these positive effects and results in the formation of brittle intermetallic phases under neutron irradiation [6–8, 25–29]. W alloys containing Cr, Ti, Y, Si have been designed to form a passive oxide layer in the event of a loss of vacuum accident, to limit oxidation and sublimation of WO<sub>3</sub> [30–39]. Addition of dopants such as potassium [15, 40], or oxide/carbide particles such as TiC, ZrC have also been

used to limit grain growth at high temperatures and reduce the DBTT [40–43].

One key challenge with developing new alloys is the wide compositional phase space, and the large number of operational conditions in which the materials are expected to perform. The use of new materials requires a good understanding of how they can be expected to perform under the full range of operational conditions, particularly under neutron irradiation. Neutron irradiation experiments are complex and require specialist equipment. Prototype alloys need to be rapidly screened for radiation tolerance before these neutron irradiation experiments are conducted. A novel approach to screening new alloys is to use composition-spread films to create samples using magnetron sputtering, which contain hundreds to thousands of different alloy compositions. In the case of sputtered composition-spread films, the physical properties of the deposited layers are sensitive to a number of deposition parameters, such as target voltage, substrate temperature and working gas pressure. Our ultimate aim is to use transient grating spectroscopy, and other rapid characterisation techniques, to screen the thermal and mechanical properties of composition spread W alloy films.

In this study we found that depositing thick W films,

---

\*matthew.lloyd@sutd.edu.sg

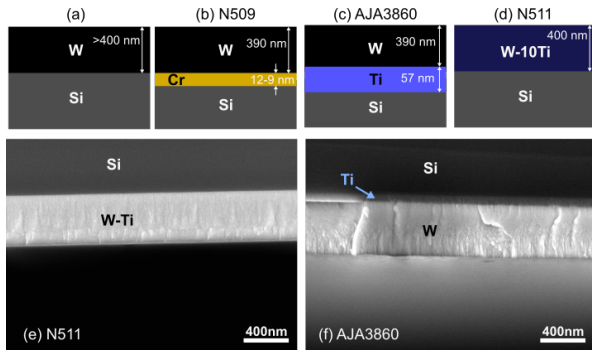


Figure 1: Schematic diagram showing the cross section of the samples investigated in this study; (a) W on Si, (b) W on Si with a Cr interlayer, (c) W on Si with a Ti interlayer and (d) W-10wt.%Ti on Si. Shown in (e) and (f) are cross-sectional SEM images of fracture surfaces in (e) W-10Ti and (f) W with Ti interlayer shown in schematic diagrams (d) and (c) respectively.

such as those required for mechanical and thermal property measurements using high throughput characterization techniques, can result in delamination from Si substrates due to the high residual stresses that develop during deposition. This delamination problem is limiting the rapid development of new W alloys by high-throughput screening with composition-spread thin films. We therefore aim to prevent delamination of the W using two approaches; using surface modification to increase interfacial adhesion between the film and substrate, and modifying the Ar gas sputtering pressure to affect the residual stresses.

Films were deposited using two magnetron sputtering systems, with 51 mm diameter metal targets of 99.95% purity, as summarised in table 2. The two systems were an AJA Orion 5, and a custom system, both of which were equipped with radio frequency sputtering guns. The custom built sputtering system consists of two AJA ST20-HV RF Magnetron Sputtering Guns mounted axially, with a target mounting block between the two guns. The guns are powered by a T&C Power Conversion Inc 0113 GTC RF Power Source, capable of outputting up to 100W at radio frequency. The AJA and custom systems achieve base chamber pressures of  $3.5 \times 10^{-5}$  Pa and  $7.3 \times 10^{-4}$  Pa respectively. The target to substrate distance was 18 cm and the substrate was not rotated during deposition which leads to lower uniformity.

The films were deposited onto Si (001) substrates which were first cleaned with acetone and isopropanol before being rinsed with deionised water and dried using compressed nitrogen. The substrates were not externally heated during deposition except by the ambient

heating due to the plasma, which was not monitored. Film thickness and composition were quantified using X-Ray Fluorescence (XRF) measurements, carried out with a Bruker M4 Tornado, Micro-XRF Spectrometer. Filterless measurements were performed using a tube voltage of 50 kV, with an emission current of  $300 \mu\text{A}$ , a spot size of  $20 \mu\text{m}$ . Specimen thicknesses were confirmed by imaging fracture surfaces with a JEOL JSM-7600F Field Emission Scanning Electron Microscope (FESEM).

W deposition was first performed directly onto Si using the AJA system at a power of 200 W, as shown schematically in figure 1 (a), giving an expected sample thickness of around 400 nm. Complete delamination of this film was observed, which prevented any further measurements of residual stress. Two samples were prepared with Cr and Ti interlayers of thickness 12 and 57 nm respectively, on top of which a W layer was deposited, as shown in figure 1 (b) and (c). Deposition powers are summarised in table 2. XRF maps were made using an analysis area of  $100 \text{ mm} \times 100 \text{ mm}$  with  $350 \times 350$  spectra, and using an acquisition spacing of  $289 \mu\text{m}$ . A pixel dwell time of 30 ms was used with a scanning speed of 9.6 mm/s.

The films deposited in the custom sputtering system have a non-uniform sample thickness, as the substrate is not rotated during deposition. The deposition profile is shown in figure 2. In the sample with a Cr interlayer, delamination of the W layer was observed, but occurred radially rather than at the point of highest W deposition. Where the W was thickest,  $380 \pm 5.6$  nm, near the centre of the specimen, delamination was prevented by the Cr interlayer, as shown in figure 1. Two regions of delamination were observed, at different Cr interlayer thicknesses. Between 10 and 11 nm, multiple fractures in the W top film produced a network of cracks where the deformed foil separated from the substrate. Where the Cr was  $< 10$  nm thick, radially propagating telephone cord delamination patterns were observed. These patterns are typically observed in films containing highly compressive residual stresses, and can be induced by a number of environmental variables [45]. W deposition under equivalent conditions was performed onto a uniform, 57 nm thick layer of Ti, that was deposited with the AJA system. In this case, the film was completely stabilised and no delamination was observed.

The residual stresses in the films were investigated using X-Ray Diffraction (XRD) and compared with other studies. Verbrugghe et. al studied W film decohesion from Si substrates before and after annealing at  $500^\circ\text{C}$  in thick W films ( $> 600 \text{ nm}$ ). De-lamination in this case was limited using the deposition of a thin

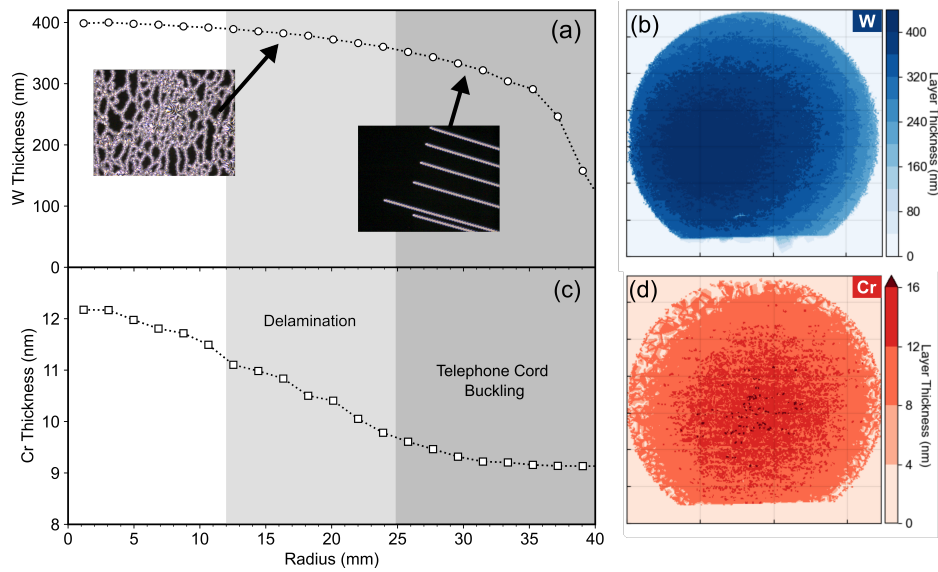


Figure 2: Maps showing the thickness of (a) W and (b) Cr measured using XRF emission of the respective layers. Plot of (c) W and (d) Cr thickness as a function of radial distance from the point of maximum Cr thickness. Inlaid are optical images taken using the XRF system showing the different delamination patterns observed at certain points on the sample. The position of peak deposition was obtained using an intensity threshold of the W  $k\text{-}\alpha$  XRF map. A radial intensity profile centred on the point of maximum intensity was calculated using the radial profile plugin for ImageJ. Figures 2 (c) and (d) show plots of the normalised integrated radial intensity as a function of radius from the point of maximum intensity for W and Cr respectively. Figure 2 (c) shows that slight misalignment of the substrate with respect to the gun results in an offset in W deposition profile, with respect to Cr. Between 0 and 10 mm from the point of highest fluoresce, deposition was uniform. Further from this point the W layer thickness decreases slightly, down to 300 nm at 25 mm due to the deposition profile of the gun.

(< 100 nm) layer of W prior to deposition of the film to both improve adhesion and reduce film stresses [46]. Various studies have also varied the deposition parameters to reduce the magnitude of residual stresses, including by using a heated substrate and a higher Ar pressure [47, 48]. Direct deposition of W onto Si was also trialled in this study, using an initial W interlayer deposited at 40 W, followed by 400 nm of W, however, delamination was not prevented.

XRD measurements were carried out in a symmetric, Bragg-Brentano, configuration in which the signal is obtained from both the film, interlayer and substrate. All measurements were performed using a Bruker D8 Discover equipped with a Cu x-ray gun producing a wavelength of 1.5418Å. Measurements were obtained in the range of  $2\theta = 10 - 120$  using an angular increment of  $0.02^\circ$ , which provides sufficient resolution to separate the  $\alpha$  and  $\beta$  W (110) peaks and calculate the lattice distortion. A strong Si (400) peak at  $69.20^\circ$  was measured, which is produced by the substrate. The position of the Si peak relative to the theoretical position was used to confirm that there was no offset in the data, and that the system was correctly aligned.

The  $\alpha$ -W (110) peak in the samples with Cr and Ti interlayers, shown in figure 3, is shifted from the expected

position, indicating that high residual stresses are still present in these samples despite the fact the delamination was prevented. High residual stresses in the film are expected for low Ar pressures deposited without substrate heating [47].

To understand how residual stresses are affected by deposition parameters, two films of W and W-10wt.%Ti were deposited directly on to Si substrates at Ar pressures of 0.5 and 2.5 Pa respectively. In both cases no visible delamination occurred after sputtering. Compressive stresses are present in the W-Ti alloy, but no delamination was observed (note that deposition of pure W at 0.5 Pa onto Si led to delamination). Deposition at 2.5 Pa led to a lower residual stress in the film, but also generated a small peak at  $2\theta = 35.25^\circ$ , corresponding to the (200) peak of  $\beta$ -W. The fraction of non-equilibrium phases after sputtering should be minimised in the current approach to accelerated alloy design, as radiation induced precipitation could also lead to the formation of non-equilibrium phases. Annealing of samples deposited in this way could be used to dissolve these phases.

To further investigate the experimental results, a systematic study based on the cohesion properties of incoherent W/Cr interfaces was carried out using first-

Table 1: The technical details of DFT calculations of W/Cr interfaces (the number of layers and atoms used for the W and Cr sub-systems) with different surface orientations and the corresponding interface binding energies from fully relaxed DFT calculations.

| W/Cr interfaces                   | (100)/(100) | (110)/(110) | (110)/(100) | (100)/(110) | (111)/(111) | (211)/(211) |
|-----------------------------------|-------------|-------------|-------------|-------------|-------------|-------------|
| W/Cr layers                       | 14/14       | 10/10       | 10/14       | 14/10       | 18/18       | 18/18       |
| W/Cr atoms                        | 56/70       | 160/200     | 160/196     | 126/160     | 144/180     | 144/180     |
| $\gamma_{BE}$ (J/m <sup>2</sup> ) | 5.31        | 5.45        | 5.30        | 4.76        | 4.12        | 4.07        |

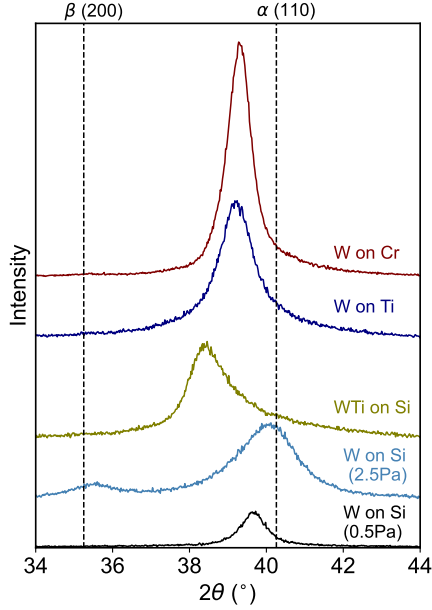


Figure 3: Portion of the XRD spectra from 5 different W and W-alloy samples deposited onto Si substrates with and without Cr/Ti interlayers, plotted between  $2\theta = 34$  and  $44^\circ$ . The theoretical position of the W  $\alpha$  (110) peak is highlighted at  $2\theta = 40.26^\circ$  [44]. The pattern from the W film at 0.5 Pa was obtained from the thinner region of the film, where delamination had not occurred. For the other samples, the measurement was taken from the centre of the sample where the thickness was around 400 nm (see table 2).

principles calculations based on the density functional theory (DFT). Technical details of our DFT calculations can be found from the previous investigations regarding on W-based high-entropy alloys (HEAs) and SMART (Self-passivating Metal Alloys with Reduced Thermo-oxidation) alloys with the presence of high-concentration of both W and Cr [37–39]. The DFT calculations were performed using the Projector Augmented Wave (PAW) method implemented in Vienna Ab-initio Simulation Package (VASP) [49–51]. Electron exchange and correlation interactions were treated within the Generalized Gradient Approximation (GGA) using Perdew, Burke and Ernzerhof (PBE) functional [52]. Total energy calculations were performed using the Monkhorst-Pack mesh of k-points [53] in the

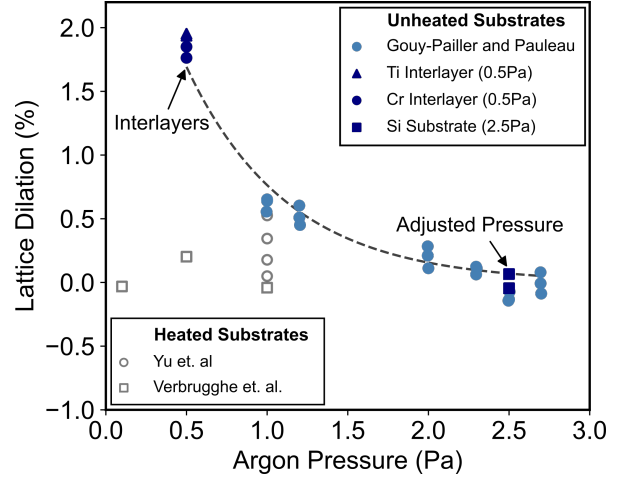


Figure 4: Lattice dilation of various peaks in sputtered W, measured using XRD [46–48]. Hollow points represent samples deposited using a heated substrate, whereas filled points were deposited at room temperature. Lattice dilation measurements for the samples measured in this study were made using the (110) and (220) peaks. An exponential curve is fit to the unheated data and is shown as a visual aid

Brillouin zone, with the k-mesh spacing of  $0.2 \text{ \AA}^{-1}$ . The plane-wave cutoff energy used in this study was set to 400 eV with the total energy convergence criterion of  $10^{-6} \text{ eV/cell}$  and force components were relaxed to  $10^{-3} \text{ eV/\AA}$ . The lattice parameters for bcc-W and bcc-Cr predicted from the present DFT studies are  $3.17 \text{ \AA}$  and  $2.84 \text{ \AA}$ , respectively. Since there are no experimental information of W/Cr interfaces, six different W/Cr configurations: W(100)/Cr(100), W(110)/Cr(100), W(110)/Cr(100), W(100)/Cr(110), W(111)/Cr(111) and W(211)/Cr(211) are considered in this study, and are shown in table 3. We use Materials Design (MeDeA) Interfaces builder [54] to create interfaces from two surfaces by allowing for certain degree of lattice mismatch between W and Cr layers. The builder provides automatic search for possible quasi-coherent interfaces and straightforward model construction for subsequent calculation of, for instance, interface energies, effect of impurities on interface strength. In this study of the interface adhesion, the optimized surfaces for W and Cr were used to generate interfaces,

with the area tolerance, length tolerance and angle tolerance each set to 5% during the interface generation stage. A large number of possible interfaces is produced, and ones with the sensible numbers of atoms for DFT calculations were selected for further analysis. Space group tolerance of the resulting interfaces was set to 0.01, while upper and lower gap were both set to 3 Å, with 0.5 ratio. Table 1 shows the number of W and Cr layers and atoms for each sub-system used in the present work for the 6 interfaces with difference Miller indices characterising the surface orientation for separated W and Cr inter-layers. In order to evaluate the adhesion stability of the interface configurations, we consider the binding energy ( $\gamma_{BE}$ ) which is the energy required to separate the interface into two free surfaces:

$$\gamma_{BE}((hkl)/(h'k'l')) = \gamma_W(hkl) + \gamma_{Cr}(h'k'l') - \gamma_{W/Cr}((hkl)/(h'k'l')) \quad (1)$$

where  $\gamma_W(hkl)$ ,  $\gamma_{Cr}(h'k'l')$  are the free surface energies for W and Cr with orientations  $(hkl)$  and  $(h'k'l')$ , respectively and  $\gamma_{W/Cr}((hkl)/(h'k'l'))$  is their interface energy. We have performed DFT calculations for the (110), (100), (111) and (211) surfaces and then used the following formula derived from [55] to calculate the average surface energy for W and Cr:

$$\gamma_{av} = \frac{1}{385}(86\gamma_{100} + 128\gamma_{110} + 27\gamma_{111} + 144\gamma_{211}) \quad (2)$$

The predicted values of  $\gamma_{av}$  are 3.49 J/m<sup>2</sup> and 3.05 J/m<sup>2</sup> for W and Cr, respectively, that are consistent with those obtained from previous DFT calculations [55, 56]. The calculated binding energies from Eq. 1 are shown in Table 1. All the calculated values of binding energy are positive demonstrating the thermodynamically stable interfaces between W and Cr for all considered surface orientations. The strongest adhesion between W and Cr is predicted for the W(110)/Cr(110) interface with the binding energy of 5.45 J/m<sup>2</sup>. Our modelling studies support the adhesion of W to Cr layers that is in agreement with the observed experimental results from this study. Taking into account the fact that Cr-rich segregation plays important role in both W-based HEAs [37–39] and in SMART alloys [30], the results of our interface W/Cr studies would have a important impact on understanding of thermodynamic stability as a function of micro-structural evolution of these materials.

To compare our findings with other studies of W films, the position of the  $\alpha$  (110) and (220) peaks were identified by fitting a Lorentzian function with a linear

background using Profex [57]. The peak shifts relative to the expected positions were used to determine the lattice dilation in the various films, and are plotted in figure 4. Figure 4, shows that decreasing Ar deposition pressure tends to increase compressive stresses, and therefore increases lattice dilation in the W films, which leads to delamination and buckling from the substrate above some critical point. Increasing the Ar pressure can reduce the stresses and prevent delamination [47]. Other studies using substrate heating have been able to use lower Ar pressures whilst maintaining low residual stresses [46, 48]. The relationship between Ar pressure and film stress is well understood in magnetron sputtering, and various studies have investigated the stress reversal phenomena in different metals. As the pressure of Ar gas in the deposition chamber increases, the energy of particles incident on the sample is reduced which prevents damage to the deposited layer [47, 58]. For W the critical point for this change from compressive to tensile stress is between 2 and 2.5 Pa, which is consistent with our findings.

In summary, delamination of W films can be prevented either by increasing surface adhesion using Ti or Cr interlayers, or by reducing residual stress development by increasing the Ar deposition pressure. These findings facilitate the growth of thick W films required for high throughput screening of W alloys. In W increasing the Ar deposition pressure leads to a higher phase fraction of the non-equilibrium  $\beta$  phase, which should be avoided for radiation screening experiments. The experimental findings were strongly supported by DFT calculations for the W-Cr interface, which showed a strong attractive interfacial energy in all of the interface orientations studied. The highest interfacial binding energy of 5.45 Jm<sup>-2</sup> was measured for the (110)/(110) interface.

## Acknowledgements

MJL, GL and RES gratefully acknowledge the SUTD-MIT International Design Centre and the Singapore Ministry of Education (MoE) for supporting this research (Grant MOE-T2EP50120-0020 Inverse design of radiation-tough high entropy alloys). DNM, JSW and DS work has been carried out within the framework of the EUROfusion Consortium, funded by the European Union via the Euratom Research and Training Programme (Grant Agreement No 101052200 — EUROfusion). Views and opinions expressed are however those of the author(s) only and do not necessarily reflect those of the European Union or the European

Commission. Neither the European Union nor the European Commission can be held responsible for them. DNM also acknowledges funding from the RCUK Energy Programme Grant No. EP/W006839/1. The work at WUT has been carried out as a part of an international project co-financed from the funds of the program of the Polish Minister of Science and Higher Education entitled "PMW" in 2019; Agreement No. 5018 / H2020-Euratom / 2019/2. The simulations were carried out with the support of the Interdisciplinary Centre for Mathematical and Computational Modelling (ICM), University of Warsaw, under grant No. GB79-6. DNM and JSW would like to thank the support from high-performing computing facility MARCONI (Bologna, Italy) provided by EUROfusion.

### Declaration of competing interest

The authors declare that they have no competing financial interests or personal relationships that could have appeared to influence the work reported in this paper

### Supplementary Information: Deposition Rates

### Supplementary Information: W-Cr Interfaces

Table 3 gives the geometries of the simulation cell used to study the W-Cr interfaces described in table 1.

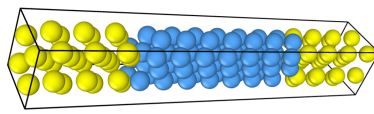
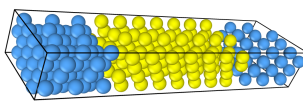
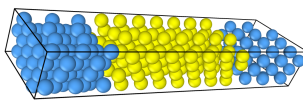
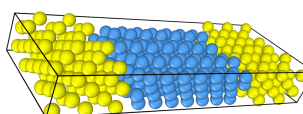
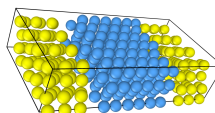
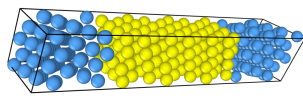
### References

- [1] D. R. Lide, CRC Handbook of Chemistry and Physics, 85th Edition, Vol. 85, CRC press, Boca Raton, FL, 2005.
- [2] H. Bolt, V. Barabash, W. Krauss, J. Linke, R. Neu, S. Suzuki, N. Yoshida, ASDEX Upgrade Team, Materials for the Plasma-Facing Components of Fusion Reactors, Journal of nuclear materials 329 (2004) 66–73.
- [3] M. Gilbert, J.-C. Sublet, S. Dudarev, Spatial Heterogeneity of Tungsten Transmutation in a Fusion Device, Nuclear Fusion 57 (4) (2017) 044002.
- [4] M. R. Gilbert, J.-C. Sublet, Handbook of Activation, Transmutation, and Radiation Damage Properties of the Elements Simulated using FISPACT-II and TENDL-2015; Magnetic Fusion Plants, Report No. CCFE-R(16)36, United Kingdom Atomic Energy Authority, Oxford, 2016.
- [5] J. C. He, G. Y. Tang, A. Hasegawa, K. Abe, Microstructural Development and Irradiation Hardening of W and W-(3–26) wt% Re Alloys after High-Temperature Neutron Irradiation to 0.15 dpa, Nuclear Fusion 46 (11) (2006) 877. doi:10.1088/0029-5515/46/11/001.
- [6] A. Hasegawa, M. Fukuda, K. Yabuuchi, S. Nogami, Neutron Irradiation Effects on the Microstructural Development of Tungsten and Tungsten Alloys, Journal of Nuclear Materials 471 (2016) 175–183. doi:10.1016/j.jnucmat.2015.10.047.
- [7] Y. Katoh, L. L. Snead, L. M. Garrison, X. Hu, T. Koyanagi, C. M. Parish, P. Edmondson, M. Fukuda, T. Hwang, T. Tanaka, et al., Response of unalloyed tungsten to mixed spectrum neutrons, Journal of Nuclear Materials 520 (2019) 193–207.
- [8] X. Hu, T. Koyanagi, M. Fukuda, Y. Katoh, L. L. Snead, B. D. Wirth, Defect Evolution in Single Crystalline Tungsten following Low Temperature and Low Dose Neutron Irradiation, Journal of Nuclear Materials 470 (2016) 278–289.
- [9] D. Papadakis, S. Dellis, V. Chatrikos, E. Manios, I. E. Stamatiatos, S. Mesoloras, K. Mergia, Neutron irradiation effects in different tungsten microstructures, Physics Scripta 96 (2021) 124041. doi:10.1088/1402-1896/ac1eb2.
- [10] S. Dellis, X. Xiao, D. Terentyev, K. Mergia, S. Krimpalis, A. Bakaev, S. Mesoloras, Mechanical properties of neutron-irradiated single crystal tungsten w(100) studied by indentation and fem modelling, Journal of Nuclear Materials 551 (2021) 152985. doi:https://doi.org/10.1016/j.jnucmat.2021.152985.
- [11] X. Hu, Recent progress in experimental investigation of neutron irradiation response of tungsten, Journal of Nuclear Materials (2022) 153856.
- [12] R. G. Abernethy, J. S. K.-L. Gibson, A. Giannattasio, J. D. Murphy, O. Wouters, S. Bradnam, L. W. Packer, M. R. Gilbert, M. Klimenkov, M. Rieth, H.-C. Schneider, C. D. Hardie, S. G. Roberts, D. E. J. Armstrong, Effects of Neutron Irradiation on the Brittle to Ductile Transition in Single Crystal Tungsten, Journal of Nuclear Materials 527 (2019) 151799.
- [13] E. Gaganidze, A. Chauhan, H.-C. Schneider, D. Terentyev, G. Borghmans, J. Aktaa, Fracture-mechanical properties of neutron irradiated ITER specification tungsten, Journal of Nuclear Materials 547 (2021) 152761.
- [14] E. Gaganidze, A. Chauhan, H.-C. Schneider, D. Terentyev, B. Rossaert, J. Aktaa, Effect of irradiation temperature on the fracture-mechanical behaviour of tungsten irradiated to 1 dpa, Journal of Nuclear Materials 556 (2021) 153200.
- [15] S. Nogami, D. Terentyev, A. Zinovev, C. Yin, M. Rieth, G. Pintsuk, A. Hasegawa, Neutron irradiation tolerance of potassium-doped and rhenium-alloyed tungsten, Journal of Nuclear Materials 553 (2021) 153009.
- [16] S. Zinkle, N. Ghoniem, Operating temperature windows for fusion reactor structural materials, Fusion Engineering and design 51 (2000) 55–71.
- [17] M. Fujitsuka, B. Tsuchiya, I. Mutoh, T. Tanabe, T. Shikama, Effect of neutron irradiation on thermal diffusivity of tungsten-rhenium alloys, Journal of nuclear materials 283 (2000) 1148–1151.
- [18] J. Habainy, Y. Dai, Y. Lee, S. Iyengar, Thermal diffusivity of tungsten irradiated with protons up to 5.8 dpa, Journal of Nuclear Materials 509 (2018) 152–157.
- [19] M. Akiyoshi, L. M. Garrison, J. W. Geringer, H. Wang, A. Hasegawa, S. Nogami, Y. Katoh, Thermal diffusivity of irradiated tungsten and tungsten-rhenium alloys, Journal of Nuclear Materials 543 (2021) 152594.
- [20] H. Gietl, T. Koyanagi, X. Hu, M. Fukuda, A. Hasegawa, Y. Katoh, Neutron irradiation-enhanced grain growth in tungsten and tungsten alloys, Journal of Alloys and Compounds 901 (2022) 163419. doi:https://doi.org/10.1016/j.jallcom.2021.163419.
- [21] P. L. Raffo, Yielding and Fracture in Tungsten and Tungsten-Rhenium Alloys, Journal of the Less Common Metals 17 (2) (1969) 133–149.
- [22] W. D. Klopp, A Review of Chromium, Molybdenum, and Tungsten Alloys, Journal of the Less Common Metals 42 (3) (1975) 261 – 278.
- [23] J. Ratliff, W. Gibeaut, H. Ogden, Tungsten Research and Development Review: 1960-1962, Vol. 193, Defense Metals Information Center, Battelle Memorial Institute, 1963.

Table 2: List of films deposited as part of this study and corresponding deposition parameters. Where no film thickness is given complete delamination of the film was observed preventing further measurements. The thickness given for the custom sputtering system correspond to measurements taken within the uniform region of maximum deposition.

| Target (wt.%) | Sputtering System | Sputtering Time (s) | Sputtering Power (W) | Deposition Rate (nm/W/s) | Ar Pressure (Pa) | Thickness (nm) |
|---------------|-------------------|---------------------|----------------------|--------------------------|------------------|----------------|
| W             | AJA Orion 5       | 3500                | 200                  | -                        | 0.5              | -              |
| W             | Custom            | 2000                | 100                  | 0.0029                   | 0.5              | 380±5.6        |
| W             | Custom            | 2000                | 100                  | 0.0029                   | 2.5              | 454±7.3        |
| Cr            | Custom            | 100                 | 50                   | 0.0019                   | 0.5              | 12             |
| Ti            | AJA Orion 5       | 1300                | 150                  | 0.0003                   | 0.5              | 57             |
| W10Ti         | Custom            | 1930                | 100                  | 0.0021                   | 0.5              | 410±6.5        |

Table 3: Table of optimised initial cell dimensions used for DFT calculations for the 6 different interfaces, prior to relaxation, and the corresponding k-points. Blue spheres represent Cr atoms and yellow represent W atoms.

| W/Cr interfaces | Cell lattice matrix (Å) |             |             | Kpoints | Figure  |
|-----------------|-------------------------|-------------|-------------|---------|---|
| (100)/(100)     | 6.39741                 | 0           | 0           | 7       |  |
|                 | 0                       | 6.39741     | 0           | 7       |   |
|                 | 0                       | 0           | 41.18325    | 1       |   |
| (110)/(110)     | 7.96475                 | 0           | 0           | 6       |  |
|                 | -3.34097812             | 14.54778009 | 1           | 3       |   |
|                 | 0                       | 0           | 42.85556    | 1       |   |
| (110)/(100)     | 7.07966                 | 0           | 0           | 7       |  |
|                 | -2.60180625             | 13.04802545 | 0           | 3       |   |
|                 | 0                       | 0           | 43.8655893  | 1       |   |
| (100)/(110)     | 6.39741                 | 0           | 0           | 7       |  |
|                 | -2.87676772             | 18.00533319 | 0           | 4       |   |
|                 | 0                       | 0           | 43.96012335 | 1       |   |
| (111)/(111)     | 7.96475                 | 0           | 0           | 6       |  |
|                 | 1.0300479               | 17.82334724 | 0           | 3       |   |
|                 | 0                       | 0           | 34.14025894 | 2       |   |
| (211)/(211)     | 9.47551                 | 0           | 0           | 5       |  |
|                 | -3.13121175             | 10.58028649 | 0           | 4       |   |
|                 | 0                       | 0           | 46.63269106 | 1       |   |

- [24] W. D. Klopp, Review of Ductilizing of Group VIA Elements by Rhenium and Other Solutes, NASA Technical Note, NASA TN D-4955, National Aeronautics and Space Administration, Washington D. C., USA, 1968.
- [25] M. Dürschnabel, M. Klimenkov, U. Jäntschi, M. Rieth, H. Schneider, Terentyev, New insights into microstructure of neutron-irradiated tungsten, *Sci. Reports.* 7 (2021) 7572. doi:10.1038/s41598-021-86746-6.
- [26] P. D. Edmondson, B. Gault, M. R. Gilbert, An Atom Probe Tomography and Inventory Calculation Examination of Second Phase Precipitates in Neutron Irradiated Single Crystal Tungsten, *Nuclear Fusion* 60 (12) (2020) 126013.
- [27] T. Hwang, A. Hasegawa, K. Tomura, N. Ebisawa, T. Toyama, Y. Nagai, M. Fukuda, T. Miyazawa, T. Tanaka, S. Nogami, Effect of Neutron Irradiation on Rhenium Cluster Formation in Tungsten and Tungsten-Rhenium Alloys, *Journal of Nuclear Materials* 507 (2018) 78–86. doi:10.1016/j.jnucmat.2018.04.031.
- [28] M. J. Lloyd, R. G. Abernethy, M. R. Gilbert, I. Griffiths, P. A. J. Bagot, D. Nguyen-Manh, M. P. Moody, D. E. J. Armstrong, Decoration of Voids with Rhenium and Osmium Transmutation Products in Neutron Irradiated Single Crystal Tungsten, *Scripta Materialia* 173 (2019) 96–100. doi:10.1016/j.scriptamat.2019.07.036.
- [29] M. Lloyd, A. London, J. Haley, M. Gilbert, C. Becquart, C. Domain, E. Martinez, M. Moody, P. Bagot, D. Nguyen-Manh, et al., Interaction of transmutation products with precipitates, dislocations and grain boundaries in neutron irradiated w, *Materialia* 22 (2022) 101370.
- [30] A. Litnovsky, F. Klein, X. Tan, J. Ertmer, J. Coenen, C. Linsmeier, J. Gonzalez-Julian, M. Bram, I. Povstugar, T. Morgan, Y. M. Gasparyan, A. Suchkov, D. Bachurina, D. Nguyen-Manh, M. G. Gilbert, D. Sobieraj, J. S. Wróbel, E. Tejado, J. Matejček, K. Zoz, H. Benz, P. Bittner, A. Reuban, Advanced self-passivating alloys for an application under extreme conditions, *Metals* 11 (2021) 1255.
- [31] A. Litnovsky, T. Wegener, F. Klein, C. Linsmeier, M. Rasinski, A. Kreter, B. Unterberg, J. Coenen, H. Du, J. Mayer, et al., Smart tungsten alloys as a material for the first wall of a future fusion power plant, *Nuclear fusion* 57 (6) (2017) 066020.
- [32] F. Klein, A. Litnovsky, T. Wegener, X. Tan, J. Gonzalez-Julian, M. Rasinski, J. Schmitz, C. Linsmeier, M. Bram, J. W. Coenen, Sublimation of advanced tungsten alloys under demo relevant accidental conditions, *Fusion engineering and design* 146 (2019) 1198–1202.
- [33] A. Calvo, C. García-Rosales, F. Koch, N. Ordás, I. Iturriza, H. Greuner, G. Pintsuk, C. Sarbu, Manufacturing and testing of self-passivating tungsten alloys of different composition, *Nuclear Materials and Energy* 9 (2016) 422–429. doi:https://doi.org/10.1016/j.nme.2016.06.002.
- [34] W. Liu, C. Ye, L. Xue, W. Zhang, Y. Yan, A self-passivating tungsten bulk composite: Effects of silicon on its oxidation resistance, *International Journal of Refractory Metals and Hard Materials* 100 (2021) 105631. doi:https://doi.org/10.1016/j.ijrmhm.2021.105631.
- [35] F. Koch, S. Köppl, H. Bolt, Self passivating w-based alloys as plasma-facing material, *Journal of nuclear materials* 386 (2009) 572–574.
- [36] T. Fu, K. Cui, Y. Zhang, J. Wang, F. Shen, L. Yu, J. Qie, et al., Oxidation protection of tungsten alloys for nuclear fusion applications: A comprehensive review, *Journal of Alloys and Compounds* 884 (2021) 161057.
- [37] O. El-Atwani, N. Li, M. Li, A. Devaraj, J. K. S. Baldwin, M. M. Schneider, D. Sobieraj, J. S. Wróbel, D. Nguyen-Manh, S. A. Maloy, E. Martinez, Outstanding radiation resistance of tungsten-based high-entropy alloys, *Sci. Adv.* 5 (3) (2019). doi:10.1126/sciadv.aav2002.
- [38] D. Sobieraj, J. S. Wróbel, T. Rygiel, K. J. Kurzydłowski, O. El Atwani, A. Devaraj, E. Martinez Saez, D. Nguyen-Manh, Chemical short-range order in derivative Cr–Ta–Ti–V–W high entropy alloys from the first-principles thermodynamic study, *Phys. Chem. Chem. Phys.* 22 (2020) 23929.
- [39] D. Sobieraj, J. Wróbel, M. R. Gilbert, A. Litnovsky, F. Klein, K. J. Kurzydłowski, D. Nguyen-Manh, Composition stability and cr-rich phase formation in w-cr-y and w-cr-ti smart alloys, *Metals* 11 (2021) 743.
- [40] D. Terentyev, M. Rieth, G. Pintsuk, J. Riesch, A. Von Muller, S. Antusch, K. Mergia, E. Gaganidze, H. C. Schneider, M. Wirtz, et al., Recent progress in the assessment of irradiation effects for in-vessel fusion materials: tungsten and copper alloys, *Nuclear Fusion* (2021).
- [41] Z. Xie, R. Liu, S. Miao, X. Yang, T. Zhang, X. Wang, Q. Fang, C. Liu, G. Luo, Y. Lian, et al., Extraordinary high ductility/strength of the interface designed bulk w-zrc alloy plate at relatively low temperature, *Scientific reports* 5 (1) (2015) 1–11.
- [42] C. Yin, D. Terentyev, T. Pardoan, A. Bakaeva, R. Petrov, S. Antusch, M. Rieth, M. Vilémová, J. Matějček, T. Zhang, Tensile properties of baseline and advanced tungsten grades for fusion applications, *International Journal of Refractory Metals and Hard Materials* 75 (2018) 153–162.
- [43] Mazher Ahmed Yar and Sverker Wahlberg and Hans Bergqvist and Hanadi G. Salem and Mats Johnsson and Mamoun Muhammed, Chemically produced nanostructured ODS–lanthanum oxide–tungsten composites sintered by spark plasma, *Journal of Nuclear Materials* 408 (2) (2011) 129–135. doi:https://doi.org/10.1016/j.jnucmat.2010.10.060.
- [44] L. Dubrovinsky, S. Saxena, Thermal expansion of periclase (mgo) and tungsten (w) to melting temperatures, *Physics and Chemistry of Minerals* 24 (8) (1997) 547–550.
- [45] P. Waters, A. Volinsky, Stress and moisture effects on thin film buckling delamination, *Experimental mechanics* 47 (1) (2007) 163–170.
- [46] N. Verbrugghe, D. Fasquelle, B. Duponchel, S. Députier, Study of tungsten films deposited by dc sputtering dedicated to integrated heaters, *Journal of Vacuum Science & Technology B, Nanotechnology and Microelectronics: Materials, Processing, Measurement, and Phenomena* 35 (3) (2017) 031204.
- [47] P. Gouy-Pailler, Y. Pauleau, Tungsten and tungsten–carbon thin films deposited by magnetron sputtering, *Journal of Vacuum Science & Technology A: Vacuum, Surfaces, and Films* 11 (1) (1993) 96–102.
- [48] J. G. Yu, W. J. Han, Z. C. Sun, K. G. Zhu, Morphology and microstructure of tungsten films by magnetron sputtering, in: *Materials Science Forum*, Vol. 913, Trans Tech Publ, 2018, pp. 416–423.
- [49] G. Kresse, J. Furthmüller, Efficient iterative schemes for ab initio total-energy calculations using a plane-wave basis set, *Phys. Rev. B* 54 (16) (1996) 11169–11186. doi:10.1103/PhysRevB.54.11169.
- [50] G. Kresse, J. Furthmüller, Efficiency of ab-initio total energy calculations for metals and semiconductors using a plane-wave basis set, *Comput. Mater. Sci.* 6 (1) (1996) 15–50. doi:10.1016/0927-0256(96)00008-0.
- [51] J. Hafner, Ab-Initio Simulations of Materials Using VASP : Density-Functional Theory and Beyond, *J. Comput. Chem.* 29 (13) (2008) 2044–2078. doi:10.1002/jcc.21057.
- [52] J. P. Perdew, K. Burke, M. Ernzerhof, Generalized gradient approximation made simple, *Phys. Rev. Lett.* 77 (18) (1996) 3865–3868. doi:10.1103/PhysRevLett.77.3865.
- [53] J. D. Pack, H. J. Monkhorst, Special points for Brillouin-

- zone integrations, *Phys. Rev. B* 13 (12) (1976) 5188–5192. doi:10.1103/PhysRevB.13.5188.
- [54] Medea and Materials Design are registered trademarks of Materials Design, Inc. <https://www.materialsdesign.com/medea-software>.
- [55] D. R. Mason, D. Nguyen-Manh, M.-C. Marinica, R. Alexander, A. E. Sand, S. L. Dudarev, Relaxation of microscopic and mesoscopic irradiation-induced defects in tungsten, *J. Appl. Phys.* 126 (2019) 075112. doi:10.1063.1.5098452.
- [56] M. P. J. Pukkinen, Q. M. Hu, S. K. Kwon, B. S. Johansson, J. Kollar, L. Vitos, Surface properties of 3d transition metals, *Philosophical Magazine A* 91 (2011) 3627–3640. doi:10.1080/14786435.2011.586953.
- [57] N. Doebelin, R. Kleeberg, Profex: a graphical user interface for the rietveld refinement program bgmn, *Journal of applied crystallography* 48 (5) (2015) 1573–1580.
- [58] D. Hoffman, J. A. Thornton, The compressive stress transition in al, v, zr, nb and w metal films sputtered at low working pressures, *Thin Solid Films* 45 (2) (1977) 387–396.